A REVIEW OF ABSORBING BOUNDARY CONDITIONS FOR TWO AND THREE-DIMENSIONAL ELECTROMAGNETIC SCATTERING PROBLEMS

R. Mittra, O. Ramahi, A. Khebir, R. Gordon and A. Kouki
Electromagnetic Communication Laboratory
University of Illinois
1406 W. Green Street
Urbana, IL 61801

Abstract

In this paper we briefly review the derivation of two- and three-dimensional absorbing boundary conditions (ABC's) for mesh truncation in PDE solution of electromagnetic scattering problems, compare the approximate 2-D ABC with its exact counterpart and suggest ways by which the ABC's can be improved. We also discuss a direct application of the Wilcox expansion to the mesh truncation problem that by-passes the ABC altogether. In addition, we address the question of using a conformal (as opposed to cylindrical) outer boundary and derive the ABC for this geometry for 2-D scattering and guided wave problems.

Introduction

Recent years have seen an increasing interest [1-6] in the solution of electromagnetic scattering problems via a direct treatment of Maxwell's equations using the finite difference (FD) and finite element (FEM) techniques, because such a direct formulation of the scattering problem appears to be especially well-suited for scatterers of complex shape and with inhomogeneous coatings. Not only is the fill-time of the matrix equation derived by using the FD or FEM approaches is substantially smaller than that in the Method of Moments (MoM) approach, but the resulting matrix is highly sparse as well and can be efficiently solved using special algorithms.

One potential disadvantage of the PDE methods applied to the solution of open region scattering problems is that an artificial outer boundary must be introduced to bound the region surrounding the scatterer that is subdivided into meshes for the purpose of discretization. Two types of boundary conditions have been used on this artificial outer boundary in order to effect the mesh truncation, viz., (i) global or nonlocal; (ii) local. The global boundary conditions are exact, but they result in a full matrix, at least insofar as the boundary nodes are concerned. In contrast, the local boundary conditions preserve the sparsity of the matrix and, consequently, are highly attractive from a numerical point of view. However, the local boundary conditions are inexact in their truncated asymptotic form and introduce errors in the solution because of the presence of reflecting waves from the outer boundary which is not totally absorbing under the constraint of these boundary conditions. The local boundary conditions are also inaccurate when traveling waves are excited on the scatterer and substantial global type of coupling exists between widely separated parts of the scatterer.

The purpose of this paper is to investigate some aspects of the local type of absorbing boundary conditions (ABC's), identify the source of errors in these conditions, and suggest possible ways for improving them.

Summary of Derivation of Local ABC's

A comprehensive discussion of various methods for deriving the local boundary conditions is beyond the scope of this work and the interested reader is referred to the papers by Bayliss, Gunzburger, and Turkel [5], Enguist and Majda [2] and Mittra and Ramahi [7] for details of three approaches to deriving the local ABC's. In this section we briefly review the derivation of the local absorbing boundary conditions for two and three-dimensional scalar and three-dimensional vector forms.

Two-Dimensional Absorbing Boundary Condition

A convenient way to derive the local ABC is to begin with the Wilcox expansion [8] for the wave function u, which is valid for large asymptotic distances ρ from the origin. The expansion can be written as

$$u \approx \frac{e^{-jk\rho}}{\sqrt{\rho}}\left(a_0(\phi)+\frac{a_1(\phi)}{\rho}+\frac{a_2(\phi)}{\rho^2}+\ldots\right) \tag{1}$$

Imposing the requirement that u satisfy the wave equation

$$\nabla^2 u + k^2 u = 0 \tag{2}$$

one can readily derive the recursion relationship

$$-2jk\,(n+1)\,a_{n+1} = \left(n+\frac{1}{2}\right)^2 a_n + D\,a_n \tag{3}$$

where $D = \partial^2/\partial\phi^2$.

Next, we use (1) to express the radial derivative of u, i.e., u_ρ as

$$u_\rho = -jk\,u - \frac{e^{-jk\rho}}{\rho^{3/2}}\sum_{n=0}^{\infty}\frac{(n+1/2)\,a_n}{\rho^n}$$

$$= \left(-jk-\frac{1}{2\rho}\right)u - \frac{e^{-jk\rho}}{\rho^{5/2}}\sum_{n=1}^{\infty}\frac{na_n}{\rho^{n-1}} \tag{4}$$

Replacing na_n in the summation in (3) using (2) we get

$$u_\rho = \left(-jk-\frac{1}{2\rho}+\frac{1}{8jk\rho^2}\right)u + \frac{1}{2jk\rho^2}Du + \frac{e^{-jk\rho}}{jk\rho^{7/2}}\sum_{n=1}^{\infty}\frac{na_n}{\rho^{n-1}} + 0\left(\frac{1}{\rho^{9/2}}\right) \tag{5}$$

Once again, replacing na_n in (4), and using the recursion relation we obtain

$$u_\rho = \left(-jk-\frac{1}{2\rho}+\frac{1}{8jk\rho^2}+\frac{1}{8k^2\rho^3}\right)u + \left(\frac{1}{2jk\rho^2}+\frac{1}{2k^2\rho^3}\right)Du + 0\left(\frac{1}{\rho^{9/2}}\right)$$

$$= \alpha(\rho)\,u + \beta(\rho)\,u_{\phi\phi} \tag{6}$$

Equation (6) can be shown to be equivalent to the one presented in [5] where a totally different derivation has been used.

The approach described above can be readily generalized to the three-dimensional scalar and vector cases. The details of the derivation have been given in [7] and only the final results are included here.

For the 3-D scalar case the asymptotic representation reads

0018-9464/89/0700-3034$01.00©1989 IEEE

$$u = \frac{e^{-jkr}}{r} \sum_{n=0}^{\infty} \frac{a_n(\theta,\phi)}{r^n} \tag{7}$$

and the absorbing boundary condition is given by

$$u_r = -jk \{\alpha(r)\, u + \beta(r)\, Du\} \tag{8}$$

where D = Beltrami's operator and Df is given by

$$Df = \frac{1}{\sin\theta} \frac{\partial}{\partial\theta} \left(\sin\theta \frac{\partial f}{\partial\theta}\right) + \frac{1}{\sin^2\theta} \frac{\partial^2 f}{\partial\phi^2} \tag{9}$$

and

$$\alpha(r) = (1 + 1/jkr);\ \beta(r) = 1/\{2(kr)^2\alpha(r)\} \tag{10}$$

up to and including terms of order r^{-4}.

For the 3-d vector case one may begin with the representation

$$\mathbf{E} = \frac{e^{-jkr}}{r} \sum_{n=0}^{\infty} \frac{\mathbf{A}_n(\theta,\phi)}{r^n} \tag{11}$$

and derive the following vector ABC

$$\nabla \times \mathbf{E} = \bar{\alpha}(r)\, E + \beta(r)\, D_4\, \mathbf{E} \tag{12}$$

where

$$\bar{\alpha}(r) = -jk \left(\hat{r} \times + \frac{1}{jkr} + \frac{D_1}{jkr}\right) \tag{13}$$

and

$$\beta(r) = \frac{1}{2jkr^2} \frac{1}{(1+1/jkr)} \tag{14}$$

An alternate derivation of the vector ABC may be found in Peterson [9] where an extension of the method described in [5] has been followed.

Comparison with the Exact Boundary Condition

In this section we will compare the ABC for the two-dimensional scalar problem, given in (6), with its exact counterpart, in order to gain an understanding of the source of the errors in the approximate ABC. The discussion below is also helpful in suggesting how we might improve the approximate ABC.

We begin with an exact representation of the scattered field, outside a cylindrical boundary circumscribing the scatterer, as follows

$$u = \sum_{n=0}^{N} a_n H_n^{(2)}(k\rho)\, e^{jn\phi} \tag{15}$$

From (15) we immediately have

$$u_\rho^{exact} = \sum_{n=0}^{N} a_n \frac{\partial H_n^{(2)}(k\rho)}{\partial\rho}\, e^{jn\phi} \tag{16}$$

Next, we compare u_ρ/u for, which we define as γ_n, for various cylinder harmonics n. We do this by deriving γ_n using the approximate ABC in (6) and its exact counterpart given by $H_n'(k\rho)/H_n(k\rho)$. Figure 1 shows this comparison for both the real and imaginary parts of γ_n, for both the second and fourth order Bayliss-Turkel (B-T) ABC operators B_2 and B_4, respectively, the latter being derivable by extending the procedure outlined earlier. The computations in Fig. 1 have been carried out for kρ=51, and are relevant for a scatterer whose ka size is less than 50; however, the calculations can easily be done for other values of kρ as well.

We note from Fig. 1 that the approximate boundary condition is quite satisfactory for the lower order harmonics up to about n=40, and then begins to deviate from the exact one for n>40. The departure from the exact γ_n is particularly noticeable for the real part of γ_n, which plays the role of the attenuation constant for the cylindrical harmonics that may be regarded as the characteristic solutions for the open cylindrical waveguides. We conclude from the above that the absorbing boundary conditions are not very accurate for evanescent or near-evanescent waves. Thus, if the scattered field at the truncation boundary has a significant contribution from either the evanescent waves or waves traveling along the boundary in the local region of interest, then errors would be introduced in the solution if the ABC is imposed in that region of the boundary.

An approach to improving this situation is to approximate the exact γ_n for a given kρ with an ascending polynomial in n^2 and then interpret the factor n^2 as being equivalent to the negative of $D = \partial^2/\partial\phi^2$. One such approximation for kρ = 50, derived by using the software called Mathematica, is given by

$$\gamma_n^{(6)} = a + b\, n^2 + c\, n^4 + d\, n^6$$

$$a = -0.019342 - j\, 0.9744$$

$$b = 6.431\times10^{-5} + j\, 2.83\times10^{-5}$$

$$c = -3.824\times10^{-8} + j\, 1.85\times10^{-7}$$

$$d = -5.158\times10^{-12} - j\, 3.242\times10^{-11} \tag{17}$$

The improvement in the approximation of γ_n, obtained via the polynomial matching approach, is shown in Fig.2.

It is also of interest to compare the improvement in the far-field results, e.g., the bistatic cross-section, obtained by using the second-order Bayliss-Turkel type of ABC, derived from the asymptotic expansion, and the one obtained by using (17). Figure 3 shows the geometry of the problem and Fig. 4 shows the results for the bistatic RCS for a circular cylinder of ka=50 when it is illuminated by a plane wave impinging upon it from the left. The improvement in the RCS results obtained by using the numerically-derived ABC is evident from Figure 4. Before closing this section, we would like to mention that the same type of improvement does not result when a higher order B-T operator is employed in place of the numerically-derived ABC. We would also like to refer to the work of Mittra and Ramahi [7] for the suggestion of an alternate approach to improving the asymptotic ABC.

Direct Application of Wilcox's Expansion

A way to bypassing the need for an ABC altogether is to use the Wilcox expansion [8] directly at the outer boundary. In this method, one extrapolates the values of the wave function external to the boundary, in terms of its values inside and on the outer nodes, by using the Wilcox's asymptotic expansion. This allows one to truncate the mesh in the finite difference (FD) or the finite element method, without spoiling the sparsity of the resulting matrices if only the second-order angular derivatives are retained in the representation. In Fig. 5 we show the geometry of the problem of scattering by a sphere to which this approach has been applied. In Fig. 6 we present some representative numerical results for the

current distribution on the sphere, obtained by enforcing the outer boundary condition *a la* Wilcox at kr = 22.4 for a sphere of ka = 16. The procedure is extremely simple to implement and has been described in detail in Mittra and Gordon [10].

Absorbing boundary condition for an Arbitrary Outer Boundary

In many problems, the geometry of the object being considered is such that using a circular or spherical outer boundary would be storage intensive and numerically inefficient, as for instance, when the body is long and slender. It would be highly desirable to choose an outer boundary that is conformal to the shape of the object as for instance in Fig. 7. An approximate boundary condition based on the asymptotic representation of the fields has been derived by Khebir et. al [11], for a two-dimensional scalar problem and an outer boundary of an arbitrary shape, using a coordinate system shown in Fig. 8. The boundary condition takes the form

$$\frac{\partial u}{\partial n} = \bar{\alpha}\, u + \bar{\gamma}\, u_t + \bar{\beta}\, u_{tt} \tag{18}$$

where

$$\bar{\alpha} = (x_0 \sin\theta_0 - y_0 \cos\theta_0)\left(-\frac{jk}{\rho} - \frac{1}{2\rho^2} - \frac{j}{8k\rho^3} + \frac{1}{8k^2\rho^4}\right) \tag{19}$$

$$\bar{\gamma} = \frac{-t\,(x_0 \sin\theta_0 - y_0 \cos\theta_0) + \frac{1}{2}\sin 2\theta_0\,(y_0^2 - x_0^2) + x_0 y_0 \cos 2\theta_0}{\rho^2} \tag{20}$$

$$\bar{\beta} = (x_0 \sin\theta_0 - y_0 \cos\theta_0)^3\left(-\frac{j}{2k\rho^3} + \frac{1}{2k^2\rho^4}\right) \tag{21}$$

where ρ is given by

$$\rho = \sqrt{t^2 + x_0^2 + y_0^2 + 2t\,(x_0\cos\theta_0 + y_0\sin\theta_0)} \tag{22}$$

where, as seen from Fig. 8, t and n are the tangent and normal to the outer boundary, respectively. In Fig. 9 we show the geometry of a thin strip which is illuminated by a plane wave at grazing incidence from the left. The oblong outer boundaries, employed in two different numerical experiments, are also shown in that figure. In the first case the vertical separation of the boundary from the surface of the strip is 1λ, whereas it is 2λ for the second case. The boundaries have semi-circular end caps of 1λ radius in both of these cases.The numerical results for the near field on the elongated boundary is shown in Figs. 10 and 11 for the two cases described above. It is seen that significant errors occur when the boundary is brought in too close to the scatterer, but that these errors go down substantially as the boundary is removed only a moderate distance away from the body.

Figure 12 shows another example of a conformal outer boundary for a wedge-shaped scatterer and Fig. 13 presents the numerical results for this case. Good agreement is found with the outer boundary only 1λ away from the scatterer. It is evident that the decrease in the number of node points is substantial for both of these objects when a conformal outer boundary is used in place of a circular outer boundary.

Application to Planar integrated Circuits

The arbitrary outer boundary concept, developed in the last section, is also useful for solving planar integrated circuits problems, e.g., microstrip lines. This has been demonstrated [12] by deriving an absorbing boundary condition for quasi-static fields an applying this boundary condition to single and coupled, n-line microstrip problems. The boundary condition again has a form identical to that in (18), but the coefficients α, β, and γ are now given by

$$\bar{\alpha} = (x_0 \sin\theta_0 - y_0 \cos\theta_0)\left(-\frac{2}{3\rho^2}\right) \tag{23}$$

$$\bar{\gamma} = \frac{-t\,(x_0 \sin\theta_0 - y_0 \cos\theta_0) + \frac{1}{2}\sin 2\theta_0\,(y_0^2 - x_0^2) + x_0 y_0 \cos 2\theta_0}{\rho^2} \tag{24}$$

$$\bar{\beta} = (x_0 \sin\theta_0 - y_0 \cos\theta_0)^3\left(\frac{1}{3\rho^2}\right) \tag{25}$$

$$\rho = \sqrt{t^2 + x_0^2 + y_0^2 + 2t\,(x_0\cos\theta_0 + y_0\sin\theta_0)} \tag{26}$$

and θ_0, x_0, y_0, and t are as shown in Fig. 8.

Numerical results have been obtained for three different microstrip geometries,viz., the single line, two-line and six-line microstrip configurations. For further details the reader is referred to [12].

References

[1] B. H. McDonald and A. Wexler, "Finite element solution of unbounded field problems," ***IEEE Trans. Microwave Theory Tech.***, vol. MTT-20, no. 12, pp. 841-847, December 1972.

[2] B. Engquist and A. Majda, "Radiation boundary conditions for the numerical simulation of waves," ***Math. Comp.***, vol. 31, no. 139, pp. 629-651, July 1977.

[3] R. MacCamy and S. Marin, "A finite element method for exterior interface problems," ***Int. J. Math. & Math. Sci.***, vol. 3, no. 2, pp. 311-350, June 1980.

[4] G. Kriegsmann and C. Morawetz, "Solving the Helmholtz Equation for Exterior Problems with Variable Index of Refraction: I," ***SIAM J. Sci. Stat.***, vol. 1, no. 3., pp. 371-385, September 1980.

[5] A. Bayliss, M. Gunzburger and E. Turkel, "Boundary conditions for the numerical solution of elliptic equations in exterior regions," ***SIAM J. Appl. Math.***, vol. 42, no. 2, pp. 430-451, April 1982.

[6] G. Meltz, B. McCartin and L. Bahrmasel, "Application of the Control Region Approximation to Electromagnetic Scattering," URSI Radio Science Meeting Program and Abstracts, p. 185, Blacksburg, Virginia, June 1987. Also submitted for publication in ***JEWA.***

[7] R. Mittra and O. M. Ramahi, "Absorbing boundary conditions for the direct solution of partial differential equations arising in electromagnetic scattering problems," ***Differential Methods in Electromagnetic Scattering***, Elsevier, NY, (to appear).

[8] C. H. Wilcox, "An expansion theorem for electromagnetic fields," ***Comm. Pure & Appl. Math.***, vol. 9, no. 2, pp. 115-134, May 1956.

[9] A. F. Peterson, "Absorbing boundary conditions for the vector wave equation," ***Microwave and Optical Technology Letters,*** vol. 1, no. 2, pp. 62-64, April 1988.

[10] R. Mittra and R. Gordon, "Radar scattering from bodies of revolution using an efficient partial differential equation algorithm," to be published in special issue of ***IEEE Trans. Antennas Propagat.***

[11] A. Khebir, O. M. Ramahi and R. Mittra, "An efficient partial differential equation method to solve complex shape scatterers," to appear.

[12] A. Khebir, A. B. Kouki and R. Mittra, "Absorbing boundary condition for quasi-TEM analysis of microwave transmission lines by the finite element method," to appear.

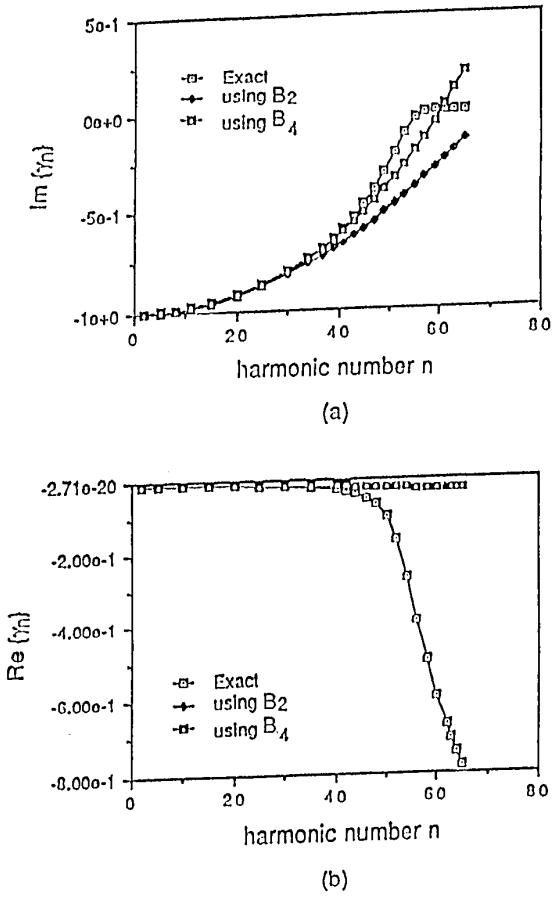

Fig. 1. γ_n as calculated using the B2 and B4 operators, and the exact γ_n, at $k\rho = 51$. (a) Imag $\{\gamma_n\}$; (b) Real $\{\gamma_n\}$

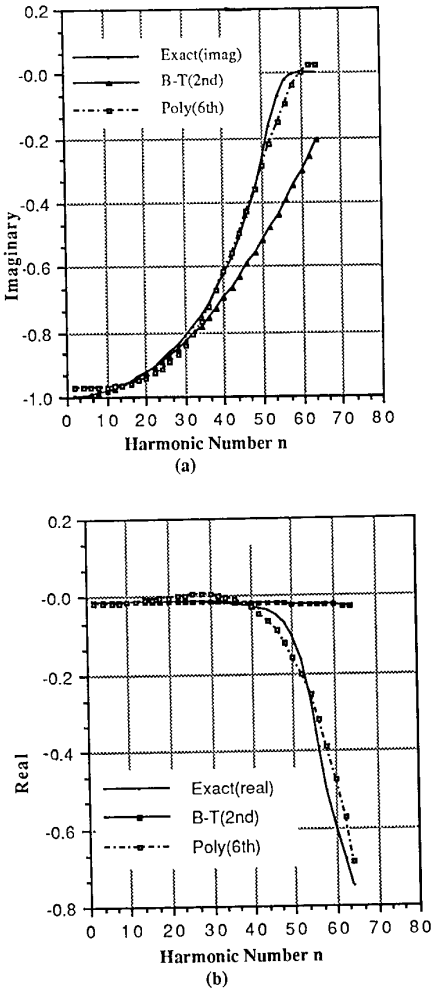

Fig. 2. Comparison of exact, B-T second order and polynomial aproximation (Poly) of γ_n . (a) Imag $\{\gamma_n\}$; (b) Real $\{\gamma_n\}$

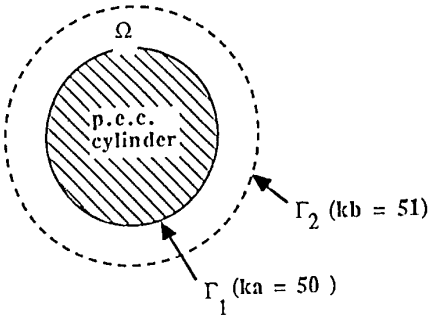

Fig. 3. Geometry of p.e.c. cylinder of size ka = 50 and artificial boundary at kb = 51

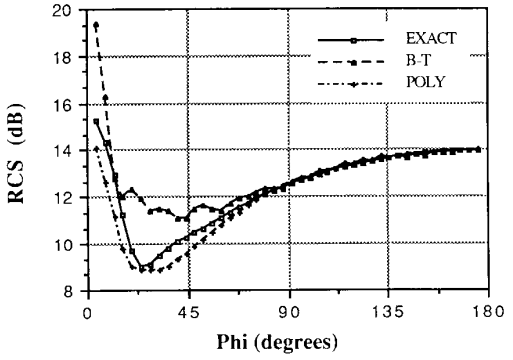

Fig. 4. Comparison of Bistatic RCS computed by using the series solution (exact), Bayliss Turkel second order (B-T) and Polynomial approximation of exact Boundary Condition (Poly). The results are for a cylinder of ka = 50, outer boundary at ka = 51 and incident field from $\phi = 180°$.

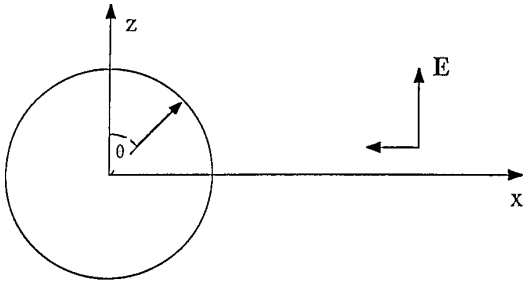

Fig. 5. Geometry of scattering problem.

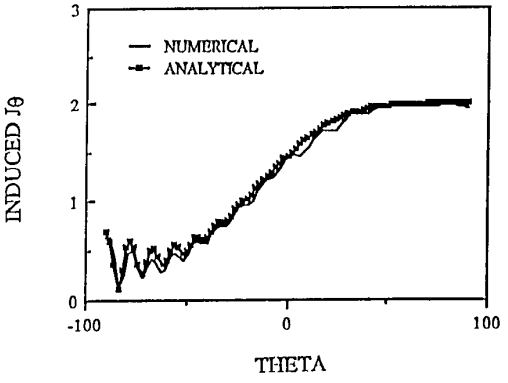

Fig. 6. Surface current density J_θ as a function of θ.

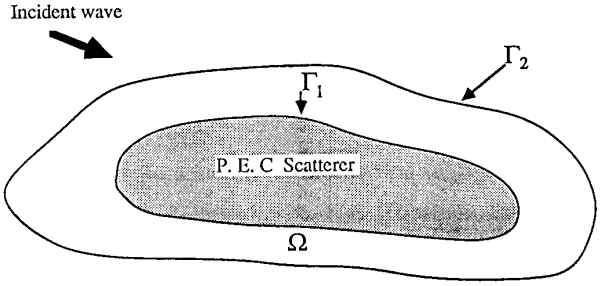

Fig. 7. Geometry for the finite-mathematics approach to the scattering problem where the scatterer and the outer boundary are both arbitrary.

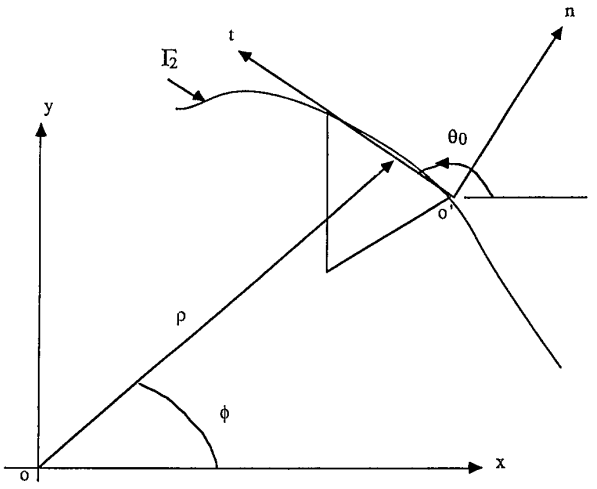

Fig. 8. A triangular element residing on the arbitrary boundary and the local coordinates of the element.

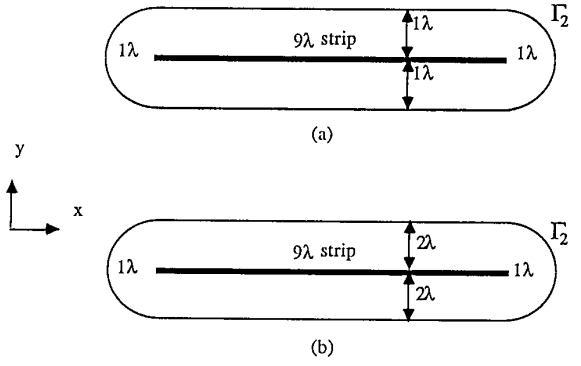

Fig. 9. A 9λ strip enclosed with an elongated boundary Γ_2.

(a) Γ_2 is 1λ away in the x- and y-directions.

(b) Γ_2 is 1λ away in x-direction and 2λ in the y-direction.

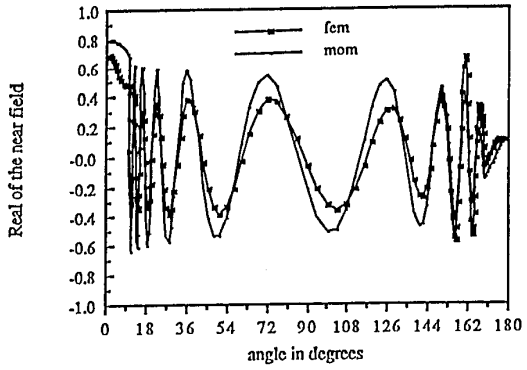

a)

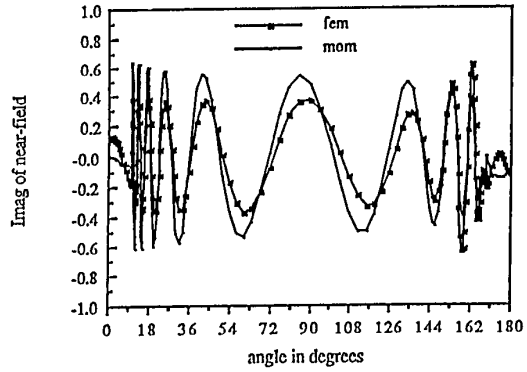

b)

Fig. 10. Near-field on the outer boundary of a 9λ strip illuminated by TM incident wave and enclosed by an elongated boundary as shown in Fig. 9a.

a) Real part of near-field, b) Imaginary part of near-field.

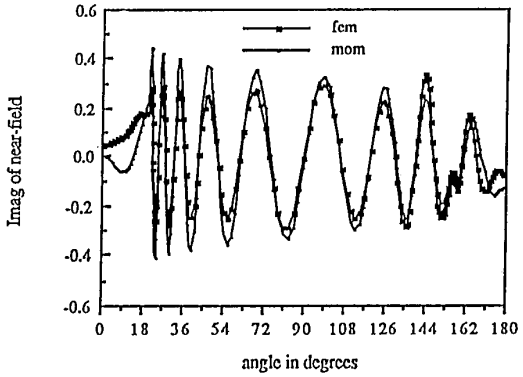

b)

Fig. 11. Near-field on the outer boundary of a 9λ strip illuminated by TM incident wave and enclosed by an elongated boundary as shown in Fig. 9b.

a) Real part of near-field, b) Imaginary part of near-field.

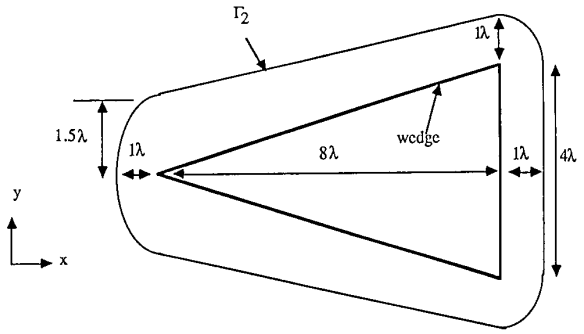

Fig. 12. An 8λ by 4λ wedge enclosed by a conformal outer boundary Γ_2.

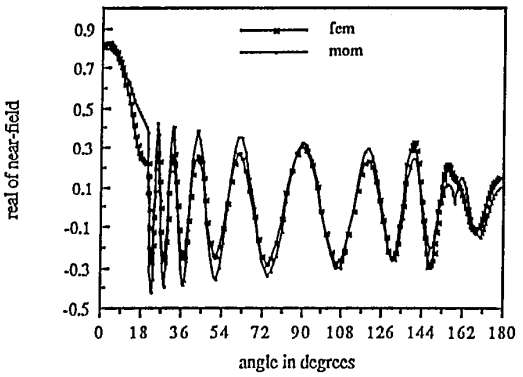

a)

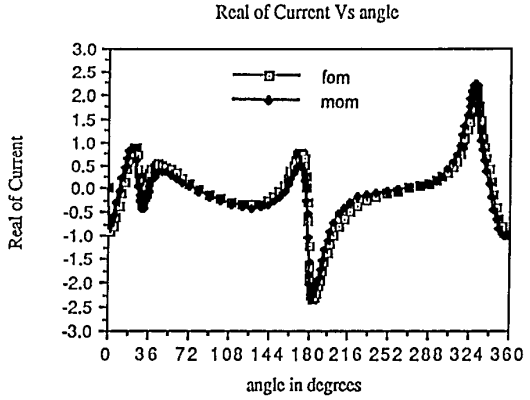

Fig. 13. Real part of the current density on a 2λ by 1λ wedge illuminated by TE incident wave and enclosed by a conformable boundary about 0.2λ away.